J. Appl. Comput. Mech., 5(5) (2019) 849-860
DOI: 10.22055/JACM.2019.27800.1435

ISSN: 2383-4536
jacm.scu.ac.ir

M&MoCS

Shahid Chamran University of Ahvaz

Journal of Applied and Computational Mechanics

Research Paper

A Paired Quasi-linearization on Magnetohydrodynamic Flow and Heat Transfer of Casson Nanofluid with Hall Effects

M. Trivedi[1], O. Otegbeye[2], Md. S. Ansari[1], S.S. Motsa[2,3]

[1] Department of Mathematics, School of Technology, Pandit Deendayal Petroleum University, Gandhinagar- 382007, India
[2] School of Mathematics, Statistics and Computer Science, University of KwaZulu-Natal, Pietermaritzburg, South Africa
[3] Department of Mathematics, University of Swaziland, Swaziland

Received December 06 2018; Revised January 24 2019; Accepted for publication March 03 2019.
Corresponding author: Md. S. Ansari, md.sharifuddin@spt.pdpu.ac.in

Abstract. Present study explores the effect of Hall current, non-linear radiation, irregular heat source/sink on magnetohydrodynamic flow of Casson nanofluid past a nonlinear stretching sheet. Viscous and Joule dissipation are incorporated in the energy equation. An accurate numerical solution of highly nonlinear partial differential equations, describing the flow, heat and mass transfer, by a new Spectral Paired Quasi-linearization method is obtained and effect of various physical parameters such as hall current parameter, radiation parameter, Eckert number, Prandtl number, Lewis number, thermophoresis parameter and Brownian motion parameter on the thermal, hydro-magnetic and concentration boundary layers are observed. The analysis shows that variation of different thermo-magnetic parameter induces substantial impression on the behaviour of temperature and nanoparticle distribution. Thermal boundary layer is greatly affected by conduction radiation parameter.

Keywords: Magnetic field, Casson Nanofluid, Mixed convection, Non-uniform heat source/sink, Paired quasi-linearization method (PQLM)

1. Introduction

The wide and varied applications of magnetic field on boundary layer flow and heat transfer which includes, Hall accelerators, refrigeration coils, MHD power generators and pumps, solar physics involved in sunspot development, the solar cycle, the structure of magnetic stars, electronic system cooling, oil extraction, thermal energy storage, flow through filtering devices and porous material regenerative heat exchangers, electrostatic precipitation, aerodynamic heating, purification of crude oils, radar systems, magnetic drug targeting and tracers, magnetic devices for cell separation etc., has been stimulating the researchers to examine the magnetohydrodynamic flow for past few decades. Turkyilmazoglu [1] studied the heat transfer characteristics with heat generation and absorption by mixed convection MHD flow of micropolar fluid past a heated or cooled stretching permeable surface. Turkyilmazoglu [2] derived an exact solution for magnetohydrodynamic viscous fluid flow and heat transfer over nonlinearly deforming surface under simultaneous impact of uniform magnetic field and internal heat generation/absorption.
Extrusion process, wire and fibre coating, polymer processing, food stuff processing, design of various heat exchangers, cooling of an infinite metallic plate in a cooling bathe, the boundary layer flow along a liquid film in condensation process, are the processes which encounter in chemical engineering field. Flow, heat and mass transfer mechanism are very important factors which determine the final quality of the product, as unidirectional orientation of the extrudate is achieved by stretching the surface. Considering the above mentioned importance, a number of researchers [3-12] reported the effect of Hall current on the magnetohydrodynamic boundary layer flow and heat transfer past a stretching surface under various conditions and geometries. Thermal conductivity of the fluids such as water, oil, ethylene glycol, bio-fluids, polymer solutions and some lubricant, etc, are

Published online: May 23 2019

improved substantially by embedding nanomaterials made of metals like copper and gold, oxides such as alumina, silica, titania and copper oxide, carbides or carbon nanotubes. Such a fluid is known as nanofluid. The notable benefits of applications of nanofluids include improved heat transfer, heat transfer system size reduction, minimal clogging, micro channel cooling, and miniaturization of systems. These interesting properties of nanofluid fascinated the researchers to investigate the flow and heat transfer characteristics. The referred research papers [13-20] explain a better insight into nanofluid flow and heat transfer. Abd el Aziz [21] reported the influence of Hall current, nano particle volume fraction and types of nanoparticle on the steady MHD flow and temperature distribution. Su and Zheng [22] presented an analysis on the flow and heat transfer of water-based nanofluids containing Copper, Silver, Alumina and Titania past a stretching wedge considering Hall effect and Joule heating. Abdel Wahed and Akl [23] considered the variation of viscosity and thermal conductivity of the fluid due to temperature and nanoparticle concentration on the MHD boundary layer flow over a rotating disk in the presence of Hall current and nonlinear thermal radiation. Makinde et al. [24] showed the significant effect of Hall current on hydromagnetic Couette Poiseuille flow of nanofluids past a rotating permeable channel. Hayat et al. [25] found the increase and decrease in velocity and fluid temperature respectively, with hall and ion slip parameter in the flow of Jeffrey nanofluids. Recently, Gireesha et al. [26] scrutinised the impact of Hall current and irregular heat generation/ consumption on two phase flow of dusty nanofluid in a stretched surface.
In this paper, we intend to study the flow and heat transfer of Casson nanofluid, a shear thinning fluid which is assumed to have an infinite viscosity at zero rate of shear, a yield stress below which no flow occurs and a zero viscosity at an infinite rate of shear [27], over a nonlinear stretching sheet together with Hall current, nonlinear radiation, irregular heat source/sink, viscous and Joule dissipation. A better insight in depth on the flow and heat transfer of Casson nanofluid can be obtained in [28 - 33]. To the best of our knowledge, such report has not appeared in literature. Present study has great significance in food processing, polymer processing industries, bio engineering operations. An accurate solution for non-dimensionalized system depicting the flow and heat transfer is obtained by Spectral Paired Quasi-linearization method.

2. Problem Statement

We analyse two-dimensional steady boundary layer flow of an incompressible, electrically conducting, heat generating/absorbing Casson nanofluid past a stretching sheet along with Joule and viscous dissipation. Fluid flow is induced due to stretching of the sheet with nonlinear velocity $U_w = ax^p$ (where $a > 0$ and p are constant). The x-axis is taken along the sheet in vertically upward direction and y- axis is taken normal to sheet. Surface of the sheet is maintained at uniform temperature $\bar{\theta}_w$ and nanoparticle concentration at surface is controlled passively [34], and $\bar{\theta}_\infty (< \bar{\theta}_w)$ and $\bar{\phi}_\infty$, are values of temperature and concentration at far away from boundary layer, respectively. A magnetic field of strength B_0 is applied normal to the sheet in the y direction which produces magnetic field effect in x direction. This causes suppression of convective flow in that direction. The induced magnetic field is ignored in comparison to applied one. Effect of Hall current actuates a cross flow and hence the flow becomes three-dimensional. Considering surface of infinite extent, a uniform variation of flow quantities in the y -direction is regarded. Generalized Ohm's law along with Hall effects is given by ([35])

$$\bar{J} + \frac{\varepsilon_e t_e}{B_0}(\bar{J} \times B) = \sigma(E^* + V \times B) \tag{1}$$

in which $\bar{J} = (\bar{J}_x, \bar{J}_y, \bar{J}_z)$ is current density vector E^* is intensity vector of electric field, V is velocity vector, ε_e is cyclotron frequency, t_e is electron collision time, σ is electrical conductivity and $B = B_0 x^{(p-1)/2}$ is magnetic induction vector. Since, no applied or polarization voltage is imposed on the flow, i.e. $E^* = 0$. Following conservation of electric current, $\bar{J}_y$ is constant and this constant is zero since $\bar{J}_y = 0$ at electrically non-conducting surface. Hence Eq. (1) reduces to $\bar{J}_x = \sigma B / (1+m^2) \times (mu - w)$ and $\bar{J}_z = \sigma B / (1+m^2) \times (u + mw)$.
Here, u, v and w represent fluid velocity along x, y and z directions, $m = \varepsilon_e t_e$ is Hall current parameter. The thermo-physical properties of the nanofluid are assumed to be constant.
Above assumptions lead the following equations describing present problem of magnetohydrodynamic steady nanofluid flow, heat and mass transfer combining simultaneous impact of hall current and internal heat generation/absorption ([36],[37] and [38]):

$$u\frac{\partial u}{\partial x} + v\frac{\partial u}{\partial y} = \upsilon\left(1+\frac{1}{\beta}\right)\frac{\partial^2 u}{\partial y^2} + \left[\left(1-\bar{\phi}_\infty\right)\rho_{f_1} g\beta_T\left(\bar{\theta}-\bar{\theta}_\infty\right) - \left(\rho_p - \rho_{f_1}\right)g\left(\bar{\phi}-\bar{\phi}_\infty\right)\right] - \frac{\sigma B}{(1+m^2)}(u+mw), \tag{2}$$

$$u\frac{\partial w}{\partial x} + v\frac{\partial w}{\partial y} = \upsilon\left(1+\frac{1}{\beta}\right)\frac{\partial^2 w}{\partial y^2} + \frac{\sigma B}{(1+m^2)}(mu - w), \tag{3}$$

$$u\frac{\partial \bar{\theta}}{\partial x} + v\frac{\partial \bar{\theta}}{\partial y} = \frac{\partial}{\partial y}\left[\left(\frac{k}{\rho c_p} + \frac{16\sigma^* \bar{\theta}^3}{3a_r \rho c_p}\right)\frac{\partial \bar{\theta}}{\partial y}\right] + \tau\left[d_B \frac{\partial \bar{\phi}}{\partial y}\frac{\partial \bar{\theta}}{\partial y} + \frac{d_\theta}{\bar{\theta}_\infty}\left(\frac{\partial \bar{\theta}}{\partial y}\right)^2\right] + \frac{Q_T}{\rho c_p} + \frac{\sigma B^2}{\rho c_p}u^2 + \frac{\upsilon}{c_p}\left(1+\frac{1}{\beta}\right)\left(\frac{\partial u}{\partial y}\right)^2, \tag{4}$$

$$u\frac{\partial\bar{\phi}}{\partial x}+v\frac{\partial\bar{\phi}}{\partial y}=d_B\frac{\partial^2\bar{\phi}}{\partial y^2}+\frac{d_\theta}{\bar{\theta}_\infty}\frac{\partial^2\bar{\theta}}{\partial y^2}. \tag{5}$$

where, $\bar{\theta}$ and $\bar{\phi}$ are dimensional fluid temperature and nanoparticle concentration, symbols β, β_T, k, σ, σ^*, a_r, υ, ρ, c_p, $(\rho c)_p$, $(\rho c)_f$, d_B and d_θ are, respectively, Casson fluid parameter, coefficient of thermal expansion, thermal conductivity, electrical conductivity, Stefan-Boltzmann constant, Rosseland mean absorption coefficient, kinematic viscosity, mass density, specific heat, effective heat capacity of the nanoparticle material, effective heat capacity of fluid, Brownian diffusion coefficient and thermophoresis diffusion coefficient and $\tau=(\rho c)_p/(\rho c)_f$.

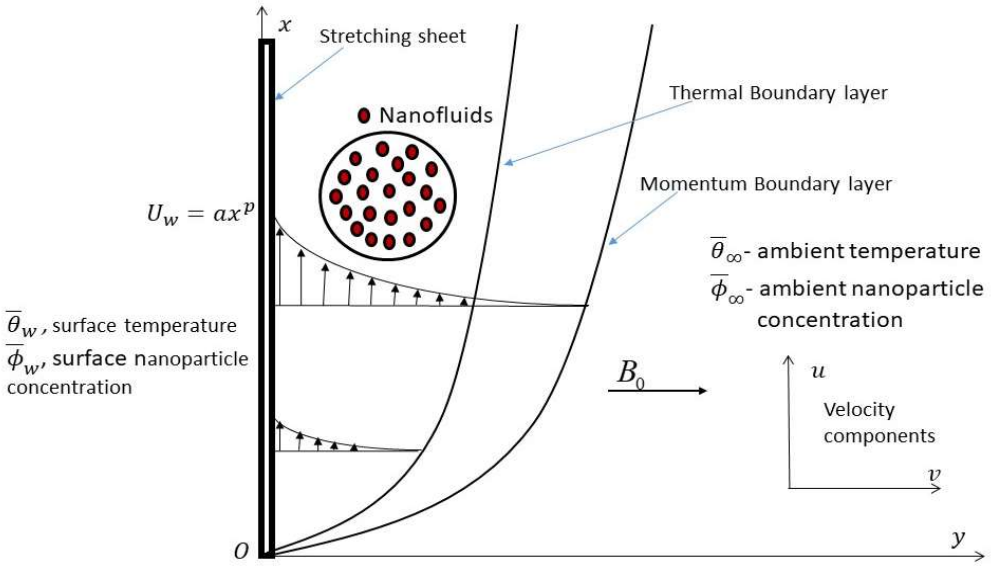

Fig. 1. Schematic diagram of the problem.

Novelty of the present study includes the Hall current, represented by last term of equations (2) and (3), the non-linear radiation, represented by second part of first term within bracket in right hand side of equation (4) and irregular heat source/sink, depicted by third last term of equation (4).

The pressure gradient and external forces are neglected in momentum equation. The boundary conditions are

$$\text{At } y=0:\ u=U_w=ax^p;\ v=-v;\ w=0;\ \bar{\theta}=\bar{\theta}_w;\ d_B\frac{\partial\bar{\phi}}{\partial y}+\frac{d_\theta}{\bar{\theta}_\infty}\frac{\partial\bar{\theta}}{\partial y}=0, \tag{6}$$

$$\text{As}\quad y\to\infty:\ u\to 0;\ w\to 0;\ \bar{\theta}=\bar{\theta}_\infty;\ \bar{\phi}=\bar{\phi}_\infty. \tag{7}$$

The irregular heat source/sink Q_T is taken as ([39])

$$Q_T=\left(\frac{kU_w}{x\upsilon}\right)[A^*(\bar{\theta}_w-\bar{\theta}_\infty)e^{-\eta}+B^*(\bar{\theta}-\bar{\theta}_\infty)], \tag{8}$$

where A^* and B^* are parameters of space-dependent and temperature-dependent heat generation/absorption. Both A^* and B^* positive corresponds to internal heat source and negative to internal heat sink. We introduce the following dimensionless variables

$$\left.\begin{aligned}
&\eta=\left(\frac{y}{x}\right)\mathrm{Re}_x^{\frac{1}{2}},\ \chi=\frac{Gr_x}{\mathrm{Re}^2},\ \psi(x,y)=\upsilon\,\mathrm{Re}_x^{\frac{1}{2}}f(\eta,\chi),\ u=\frac{\upsilon\,\mathrm{Re}_x}{x}\frac{\partial f}{\partial\eta},\\
&v=\frac{\upsilon\,\mathrm{Re}_x^{\frac{1}{2}}}{x}\left\{\frac{1+p}{2}f-\frac{1-p}{2}\eta\frac{\partial f}{\partial\eta}+(1-2p)\chi\frac{\partial f}{\partial\chi}\right\},\\
&w=\frac{\upsilon\,\mathrm{Re}_x}{x}\frac{\partial h}{\partial\eta},\quad \theta(\eta,\chi)=\frac{(\bar{\theta}-\bar{\theta}_\infty)}{(\bar{\theta}_w-\bar{\theta}_\infty)},\quad \phi(\eta,\chi)=\frac{(\bar{\phi}-\bar{\phi}_\infty)}{(\bar{\phi}_w-\bar{\phi}_\infty)}.
\end{aligned}\right\} \tag{9}$$

where, $f(\eta,\chi)$ is stream function, $h(\eta,\chi)$ is dimensionless secondary velocity, $\theta(\eta,\chi)$ is dimensionless temperature, $\phi(\eta,\chi)$ is dimensionless concentration function. The parameters χ and η are the similarity variables, $\mathrm{Re}_x=U_w x/\upsilon$ is the local Reynolds

number and $Gr_x = \{(1-\bar{\phi})\rho_{f_1} g \beta_T (\bar{\theta}_w - \bar{\theta}_\infty)\} / (\rho_f \upsilon^2)$ is the local Grashof number. Eqns. (2)-(5), under the transformation (9), take the form

$$\left(1+\frac{1}{\beta}\right)\frac{\partial^3 f}{\partial \eta^3}+\left(\frac{1+p}{2}\right) f\frac{\partial^2 f}{\partial \eta^2}-(1-2p)\chi\left(\frac{\partial^2 f}{\partial \chi \partial \eta}\frac{\partial f}{\partial \eta}-\frac{\partial^2 f}{\partial \eta^2}\frac{\partial f}{\partial \chi}\right)-p\left(\frac{\partial f}{\partial \eta}\right)^2+\chi(\theta-Nr\phi)-\frac{M}{(1+m^2)}\left(\frac{\partial f}{\partial \eta}+mh\right)=0, \tag{10}$$

$$\left(1+\frac{1}{\beta}\right)\frac{\partial^2 h}{\partial \eta^2}+\left(\frac{1+p}{2}\right) f\frac{\partial h}{\partial \eta}-(1-2p)\chi\left(\frac{\partial h}{\partial \chi}\frac{\partial f}{\partial \eta}-\frac{\partial h}{\partial \eta}\frac{\partial f}{\partial \chi}\right)-ph\left(\frac{\partial f}{\partial \eta}\right)+\frac{M}{(1+m^2)}\left(m\frac{\partial f}{\partial \eta}-h\right)=0, \tag{11}$$

$$\begin{aligned}&\frac{\partial^2 \theta}{\partial \eta^2}+\frac{4}{3Rd}\frac{\partial}{\partial \eta}\left[(\delta\theta+1)^3\frac{\partial \theta}{\partial \eta}\right]+\Pr\left(Nb\frac{\partial \phi}{\partial \eta}\frac{\partial \theta}{\partial \eta}+Nt\left(\frac{\partial \theta}{\partial \eta}\right)^2\right)+A^* e^{-\eta}+B^*\theta+\left(\frac{1+p}{2}\right)\Pr f\frac{\partial \theta}{\partial \eta}\\&-\Pr(1-2p)\chi\left(\frac{\partial f}{\partial \eta}\frac{\partial \theta}{\partial \chi}-\frac{\partial \theta}{\partial \eta}\frac{\partial f}{\partial \chi}\right)+\Pr Ec\left[M\left(\frac{\partial f}{\partial \eta}\right)^2+\left(1+\frac{1}{\beta}\right)\left(\frac{\partial^2 f}{\partial \eta^2}\right)^2\right]=0,\end{aligned} \tag{12}$$

$$\frac{\partial^2 \phi}{\partial \eta^2}+\left(\frac{1+p}{2}\right)Lef\frac{\partial \phi}{\partial \eta}+\frac{Nt}{Nb}\frac{\partial^2 \theta}{\partial \eta^2}-Le(1-2p)\chi\left(\frac{\partial f}{\partial \eta}\frac{\partial \phi}{\partial \chi}-\frac{\partial \phi}{\partial \eta}\frac{\partial f}{\partial \chi}\right)=0, \tag{13}$$

and translated boundary conditions are

$$\frac{\partial f}{\partial \eta}(0,\chi)=1,\quad f(0,\chi)=0,\quad h(0,\chi)=0,\quad \theta(0,\chi)=1,\quad Nb\frac{\partial \phi(0,\chi)}{\partial \eta}+Nt\frac{\partial \theta(0,\chi)}{\partial \eta}=0, \tag{14}$$

$$\frac{\partial f}{\partial \eta}(\infty,\chi)\to 0,\quad h(\infty,\chi)\to 0,\quad \theta(\infty,\chi)\to 0,\quad \phi(\infty,\chi)\to 0. \tag{15}$$

where,

$$\left.\begin{aligned}&M=\sigma B_0^2/a\rho,\quad \Pr=\upsilon/a,\quad Nb=\tau d_B\left(\bar{\phi}_w-\bar{\phi}_\infty\right)/\upsilon,\\&Nt=\tau d_\theta\left(\bar{\theta}_w-\bar{\theta}_\infty\right)/\upsilon\bar{\theta}_\infty,\quad Le=\upsilon/d_B,\quad Ec=U_w^2/c_p\left(\bar{\theta}_w-\bar{\theta}_\infty\right),\\&Nr=\left(\rho_p-\rho_{f_1}\right)\left(\bar{\phi}_w-\bar{\phi}_\infty\right)/\rho_{f_1}\beta_T\left(\bar{\theta}_w-\bar{\theta}_\infty\right)\left(1-\bar{\phi}_\infty\right),\\&\alpha=k/\rho c_p,\quad Rd=ka_r/4\sigma^*\bar{\theta}_\infty^3,\quad \theta_w=\bar{\theta}_w/\bar{\theta}_\infty,\quad \delta=\theta_w-1.\end{aligned}\right\}$$

are the governing parameters and M, Pr, Nb, Nr, Nt, Le, Rd and $\theta_w(>1)$ are respectively, magnetic parameter, Prandtl number, Brownian motion parameter, buoyancy ratio, thermophoresis parameter, Lewis number, conduction-radiation parameter and surface temperature excess ratio. The local skin friction coefficient Cf_x, the local Nusselt number Nu_x and the local Sherwood number Sh_x, are defined as:

$$\begin{aligned}&Cf_x\,\mathrm{Re}_x^{\frac{1}{2}}=\left(1+\frac{1}{\beta}\right)\left.\frac{\partial^2 f}{\partial \eta^2}\right|_{\eta=0},\\&Nu_x\,\mathrm{Re}_x^{-\frac{1}{2}}=-\left(1+\frac{4}{3Rd}\theta_w^3\right)\left.\frac{\partial \theta}{\partial \eta}\right|_{\eta=0},\\&Sh_x\,\mathrm{Re}_x^{-\frac{1}{2}}=-\left.\frac{\partial \phi}{\partial \eta}\right|_{\eta=0}.\end{aligned}$$

3. Method of Solution

In this section, we discuss the implementation of the paired quasi-linearization method (PQLM), recently introduced by Motsa and Animasaun [40] and Otegbeye and Motsa [41], on the system of partial differential equations (10) - (15). The PQLM draws on the concept of quasi-linearization [42] that seeks to linearize a system of nonlinear equations by applying Taylor series expansion before collocating and solving the linearized system. The innovation of the PQLM however, lies in decoupling a large coupled system into pairs of equations so as to reduce the size of matrices that are to be inverted thereby minimizing computational cost. In this regard, we observe that derivatives of θ and ϕ are coupled in one of the boundary conditions so the

PQLM is a suitable method and we will pair θ and ϕ while f and h will be the initial pairing. We begin by applying quasi-linearization on f and h and their corresponding derivatives in equations (the first two equations). This gives the pair

$$\begin{aligned}
&\alpha_1 f'''_{r+1} + [a_1] f''_{r+1} + [a_2] f'_{r+1} + [a_3] f_{r+1} + (-\alpha_3 m) h_{r+1} = [a_4] \frac{\partial f'_{r+1}}{\partial \chi} + [a_5] \frac{\partial f_{r+1}}{\partial \chi} + a_6, \\
&[b_1] f'_{r+1} + [b_2] f_{r+1} + \alpha_1 h''_{r+1} + [b_3] h'_{r+1} + [b_4] h_{r+1} = [b_5] \frac{\partial f_{r+1}}{\partial \chi} + [b_6] \frac{\partial h_{r+1}}{\partial \chi} + b_7,
\end{aligned} \tag{16}$$

where $[a_i]$, $i = 1,...,5$ and $[b_i]$, $i = 1,...,6$ are vector representations and terms defined at r and $r + 1$ denote the previous and current iteration levels, respectively and

$$\begin{aligned}
&\alpha_1 = 1 + \frac{1}{\beta}, \ \alpha_2 = \frac{1+p}{2}, \ \alpha_3 = \frac{M}{1+m^2}, \ \alpha_4 = \frac{4}{3Rd}, \\
&a_1 = \alpha_2 f_r + (1-2p)\chi \frac{\partial f_r}{\partial \chi}, \ a_2 = -2pf'_r - (1-2p)\chi \frac{\partial f'_r}{\partial \chi}, \\
&a_3 = \alpha_2 f''_r, \quad a_4 = (1-2p)\chi f'_r, \ a_5 = -(1-2p)\chi f''_r, \\
&a_6 = \alpha_2 f_r f''_r - p(f'_r)^2 - (1-2p)\chi \left(f'_r \frac{\partial f'_r}{\partial \chi} - f''_r \frac{\partial f_r}{\partial \chi} \right) - \chi(\theta_r - Nr\phi_r), \\
&b_1 = -ph_r - (1-2p)\chi \frac{\partial h_r}{\partial \chi} + \alpha_3 m, \quad b_2 = \alpha_2 h'_r, \quad b_3 = \alpha_2 f_r + (1-2p)\chi \frac{\partial f_r}{\partial \chi}, \\
&b_4 = -pf'_r - \alpha_3, \quad b_5 = -(1-2p)\chi h'_r, \quad b_6 = (1-2p)\chi f'_r, \\
&b_7 = \alpha_2 f_r h'_r - ph_r f'_r - (1-2p)\chi \left(f'_r \frac{\partial h_r}{\partial \chi} - h'_r \frac{\partial f_r}{\partial \chi} \right).
\end{aligned}$$

Updated solutions for f, h and their corresponding derivatives are used in the second pair of equations while θ, ϕ and their corresponding derivatives are linearized and we obtain the pair

$$\begin{aligned}
&[c_1]\theta''_{r+1} + [c_2]\theta'_{r+1} + [c_3]\theta_{r+1} + [c_4]\phi'_{r+1} = [c_5]\frac{\partial \theta_{r+1}}{\partial \chi} + c_6, \\
&\frac{Nt}{Nb}\theta''_{r+1} + \phi''_{r+1} + [e_1]\phi'_{r+1} = [e_2]\frac{\partial \phi_{r+1}}{\partial \chi},
\end{aligned} \tag{17}$$

The linearized pairs (16) and (17) are solved using the Chebyshev spectral method [43]-[45]. To achieve this we transform the pairs from domains $\eta \in [0, \eta_\infty]$ and $\chi \in [0, \chi_\infty]$ to $\bar{x}, \bar{y} \in [-1,1]$, respectively, where η_∞ and χ_∞ are fixed constants. We assume the approximate solutions are defined using bivariate Lagrange interpolation polynomials of the form

$$E(\eta, \chi) \approx \sum_{i=0}^{M_{\bar{x}}} \sum_{j=0}^{M_{\bar{y}}} E(\bar{x}_i, \bar{y}_j) L_m(\bar{x}) L_j(\bar{y}), \qquad E = f, h, \theta, \phi. \tag{18}$$

which interpolates $E(\eta, \chi)$ at $\bar{x}_i$ and $\bar{y}_j$ where

$$\bar{x}_i = \cos\left(\frac{\pi i}{M_{\bar{x}}}\right), \ \bar{y}_j = \cos\left(\frac{\pi j}{M_{\bar{y}}}\right), \quad i = 0,1,...,M_{\bar{x}}, \quad j = 0,1,...,M_{\bar{y}}$$

are Gauss-Lobatto collocation points. The derivatives of unknown functions from pairs (16) and (17) are represented using the Chebyshev spectral method in the form

$$\begin{aligned}
&\left.\frac{\partial^m E}{\partial \eta^m}\right|_{(\bar{x}_k, \bar{y}_i)} = \boldsymbol{D}^m \boldsymbol{E}_i, \quad m = 1,2,3 \\
&\left.\frac{\partial E}{\partial \chi}\right|_{(\bar{x}_k, \bar{y}_i)} = \sum_{j=0}^{M_{\bar{y}}} \boldsymbol{d}_{ij} \boldsymbol{F}_j,
\end{aligned} \tag{19}$$

where $\boldsymbol{D} = (2/\eta_\infty)D_{l,k}$, $l,k = 0,...,M_{\bar{x}}$, with $D_{l,k}$ being a differentiation matrix with dimension $(M_{\bar{x}}+1)\times(M_{\bar{x}}+1)$. Also, $\boldsymbol{d} = 2/\chi_\infty \times d_{h,q}$, $h,q = 0,...,M_{\bar{y}}$, with $d_{l,k}$ being a differentiation matrix with dimension $(M_{\bar{y}}+1)\times(M_{\bar{y}}+1)$ and $\boldsymbol{E}_i$ being a vector defined thus

$$\boldsymbol{E}_i = \left[E_i\left(\bar{x}_0\right), E_i\left(\bar{x}_1\right), ..., E_i\left(\bar{x}_{M_{\bar{x}}}\right)\right]^T. \tag{20}$$

Applying spectral method on our linearized pairs (16) and (17), we obtain

$$\begin{aligned}
&\boldsymbol{A}_{11,i}\boldsymbol{F}_{r+1,i} + \boldsymbol{A}_{12,i}\boldsymbol{H}_{r+1,i} - \left[\mathbf{a}_{4,i}\right]\sum_{j=0}^{M_{\bar{y}}}\boldsymbol{d}_{i,j}\boldsymbol{D}\boldsymbol{F}_{r+1,j} - \left[\mathbf{a}_{5,i}\right]\sum_{j=0}^{M_{\bar{y}}}\boldsymbol{d}_{i,j}\boldsymbol{F}_{r+1,j} = \mathbf{R}_{1,i}\\
&\boldsymbol{A}_{21,i}\boldsymbol{F}_{r+1,i} + \boldsymbol{A}_{22,i}\boldsymbol{H}_{r+1,i} - \left[\mathbf{b}_{5,i}\right]\sum_{j=0}^{M_{\bar{y}}}\boldsymbol{d}_{i,j}\boldsymbol{F}_{r+1,j} - \left[\mathbf{b}_{6,i}\right]\sum_{j=0}^{M_{\bar{y}}}\boldsymbol{d}_{i,j}\boldsymbol{H}_{r+1,j} = \mathbf{R}_{2,i}
\end{aligned} \tag{21}$$

and

$$\begin{aligned}
&\boldsymbol{B}_{11,i}\Theta_{r+1,i} + \boldsymbol{B}_{12,i}\Phi_{r+1,i} - \left[\boldsymbol{c}_{5,i}\right]\sum_{j=0}^{M_{\bar{y}}}\boldsymbol{d}_{i,j}\Theta_{r+1,j} = \mathbf{R}_{3,i}\\
&\boldsymbol{B}_{21,i}\Theta_{r+1,i} + \boldsymbol{B}_{22,i}\Phi_{r+1,i} - \left[\boldsymbol{e}_{2,i}\right]\sum_{j=0}^{M_{\bar{y}}}\boldsymbol{d}_{i,j}\Phi_{r+1,j} = \mathbf{R}_{4,i}
\end{aligned} \tag{22}$$

where

$$\begin{aligned}
&\boldsymbol{A}_{11,i} = \alpha_1\boldsymbol{D}^3 + \left[\mathbf{a}_{1,i}\right]\boldsymbol{D}^2 + \left[\mathbf{a}_{2,i}\right]\boldsymbol{D} + \left[\mathbf{a}_{3,i}\right], \quad \boldsymbol{A}_{12,i} = \left(-\alpha_3 m\right)\boldsymbol{I},\\
&\boldsymbol{A}_{21,i} = \left[\mathbf{b}_{1,i}\right]\boldsymbol{D} + \left[\mathbf{b}_{2,i}\right], \quad \boldsymbol{A}_{22,i} = \alpha_1\boldsymbol{D}^2 + \left[\mathbf{b}_{3,i}\right]\boldsymbol{D} + \left[\mathbf{b}_{4,i}\right],
\end{aligned} \tag{23}$$

$$\begin{aligned}
&\boldsymbol{B}_{11,i} = \left[\mathbf{c}_{1,i}\right]\boldsymbol{D}^2 + \left[\mathbf{c}_{2,i}\right]\boldsymbol{D} + \left[\mathbf{c}_{3,i}\right], \quad \boldsymbol{B}_{12,i} = \left[\mathbf{c}_{4,i}\right]\boldsymbol{D},\\
&\boldsymbol{B}_{21,i} = \left(\frac{Nt}{Nb}\right)\boldsymbol{D}^2, \quad \boldsymbol{B}_{22,i} = \boldsymbol{D}^2 + \left[\mathbf{e}_1\right]\boldsymbol{D},
\end{aligned} \tag{24}$$

where $\boldsymbol{I}$ is an identity matrix of size $(M_{\bar{x}}+1)\times(M_{\bar{x}}+1)$.

4. Results and Discussions

To generate the numerical solution, we used 40 grid points in η direction and 10 grid points in χ directions, these values are observed to be adequate in giving accurate solution. Figures 1-8 are sketched to analyse the convergence and accuracy of the numerical scheme mentioned above $\chi = 0.5$, $M = 5$, $m = 0.5$, $\beta = 0.5$, $p = 0.3$, $\delta = 0.5$, $Pr = 15$, $Nr = 0.5$, $Nb = 0.5$, $Nt = 0.5$, $A^* = 0.5$, $B^* = 0.5$, $Ec = 0.1$, $Le = 5$ and $Rd = 0.2$. Figures 2-9 reflect the solution error norm. This has been calculated by the difference between solutions obtained in successive iterations. We observe from Fig. 2 to 5 that, the error reduces to a tolerance level 10^{-11} in 30 iterations. This shows that our iteration scheme converges. Figures 6 to 9 show the residual error, obtained by substituting the approximate solutions in original system of eqns. (10) to (13). Residual error apprise us the closeness of our solutions to analytical solution of the system.

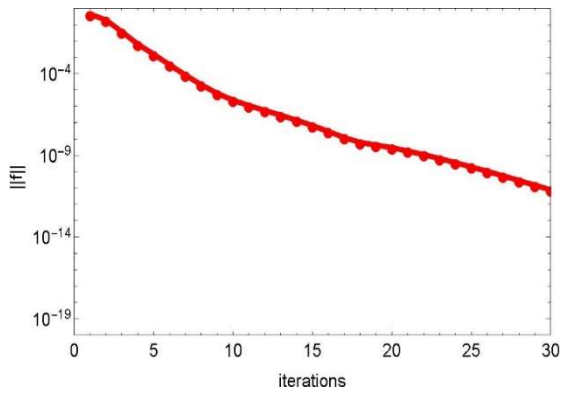

Fig. 2. Error of *f*.

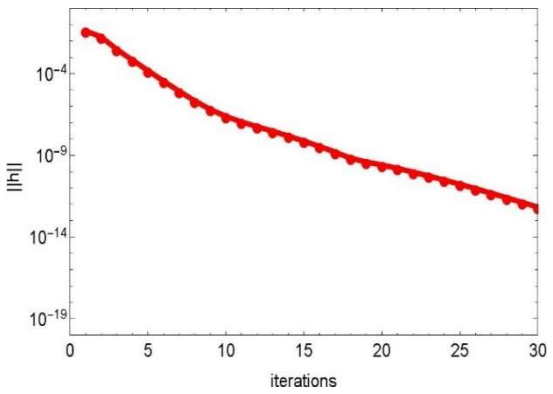

Fig. 3. Error of *h*.

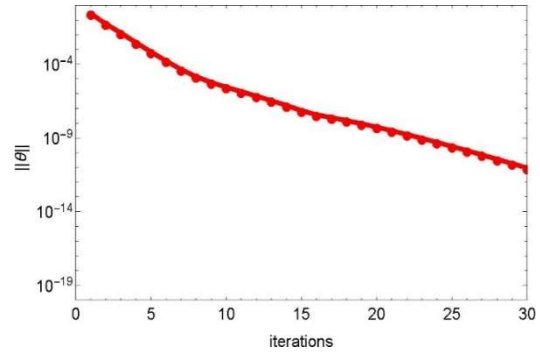

Fig. 4. Error of θ.

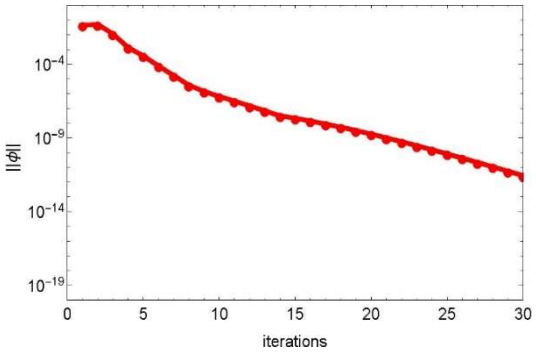

Fig. 5. Error of ϕ.

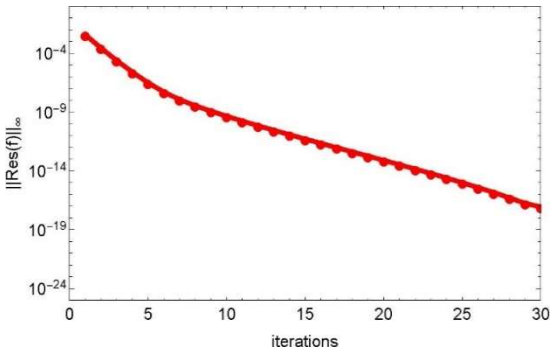

Fig. 6. Residual of f.

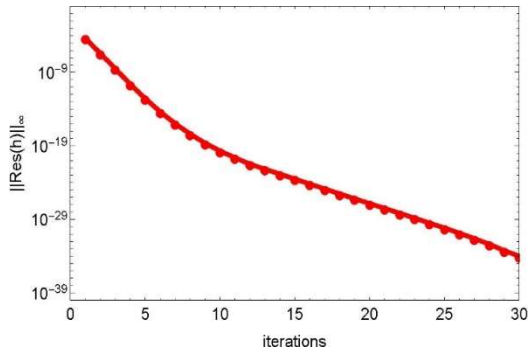

Fig. 7. Residual of h.

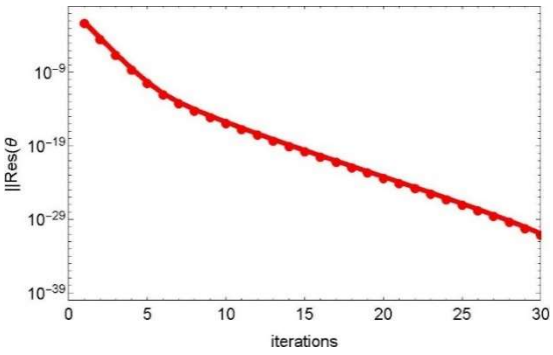

Fig. 8. Residual of θ.

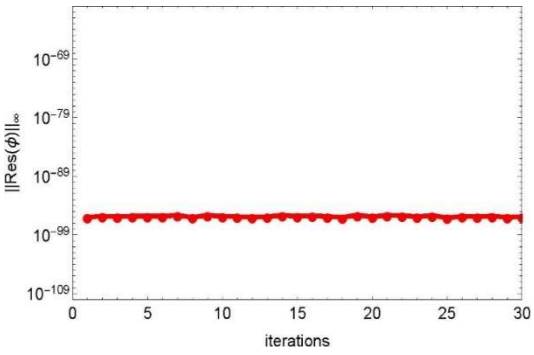

Fig. 9. Residual of ϕ.

This section analyses the effects of Hall current parameter m, Casson parameter β, radiation parameter Rd, Prandtl number Pr and Eckert number Ec on the hydromagnetic, thermal and concentration boundary layers, utilizing the value of parameters characterizing the fluid of practical interest. Figures 10 to 13 witness the behaviour of primary velocity $f'(\eta,\chi)$, secondary velocity $h(\eta,\chi)$, temperature $\theta(\eta,\chi)$ and nanoparticle concentration $\phi(\eta,\chi)$ with the variations of m. Higher values of m decrease the effective conductivity $[\sigma/(1+m^2)]$ which, reduces the magnetic damping force on primary velocity $f'(\eta,\chi)$ and this reduction results in an assisting effect on primary velocity. This effect is clearly visualized in Fig. 10. It is well known that Hall current induces secondary flow in flow region, hence secondary flow is induced and increases with m (Fig. 11). Hall current decreases the fluid temperature and maximum temperature occurs at very near to the surface. Increasing m leads to a slight decrease in nanoparticle concentration in fluid, as mentioned, augmentation of m increases the primary as well as secondary velocity. The non-dimensional concentration profiles, $\phi(\eta,\chi)$, at the surface are negative. The negative values of $\phi(\eta,\chi)$ reflect that the volume fraction of nanoparticles at the surface is lower than the free stream volume fraction of nanoparticles.

Modification of flow, thermal and concentration pattern with Casson parameter β are presented in Figs. 14-17, when $M=5$, $Pr=15$, $Rd=0.2$, $m=0.5, p=0.3$, $Nt=Nb=0.5$, $A^*=B^*=0.5$, $Le=5$, $Nr=0.5, \delta=0.5, Ec=0.1$ and $\chi=0.5$. Primary velocity decreases whereas secondary velocity increases near the surface and changes it's characteristics at far away from the surface with an increase in β. A rapid increase in secondary velocity near the stretching surface is observed. After attaining a peak it decreases to free stream. There is a gain in fluid temperature and nanoparticle concentration with β. Higher values of β correspond more plasticity of the fluid i.e. reduction in yield stress and thus, fluid experience a resistance. From Eq. (12), we see

that the effect of radiation is inversely proportional to the conduction radiation parameter Rd. Hence, small values of Rd signify a large radiation effect while $Rd \to \infty$ correspond to zero radiation. Figure 18 is plotted to visualize the impact of conduction radiation parameter Rd on temperature field when $M = 4$, $Pr = 12$, $\beta = 0.5$, $m = 0.5$, $p = 0.3$, $Nt = Nb = 0.5$, $Le = 5$, $A^* = B^* = 0.5$, $Nr = 0.5$, $\delta = 0.5$, $Ec = 0.05$ and $\chi = 0.5$. The fluid temperature is highly influenced by radiation. The fluid temperature decreases with the increase in conduction radiation parameter. This change in fluid temperature is very small for large conduction radiation parameter.

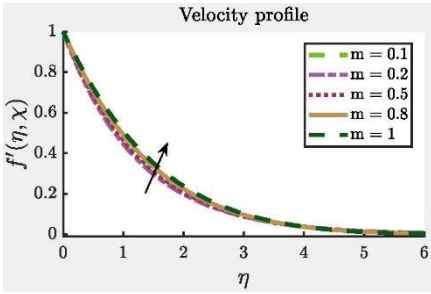

Fig. 10. Profiles of f' for different m.

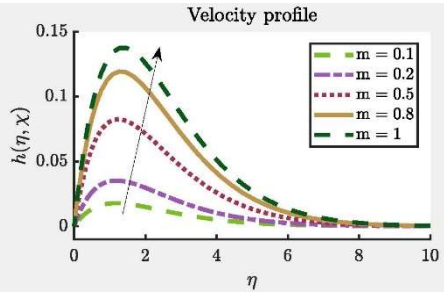

Fig. 11. Profiles of h for different m.

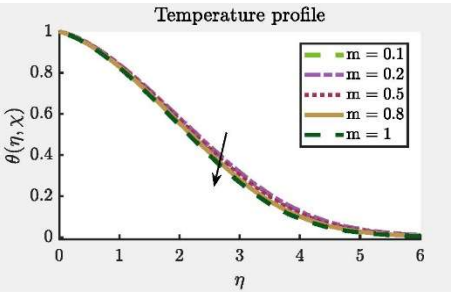

Fig. 12. Profiles of θ for different m.

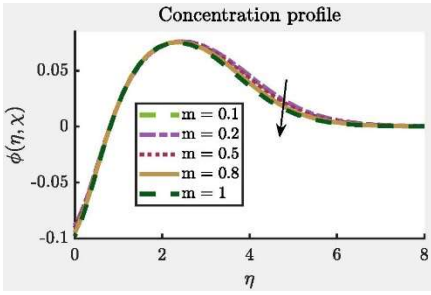

Fig. 13. Profiles of ϕ for different m.

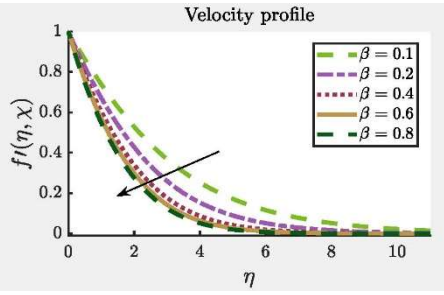

Fig. 14. Profiles of f' for different β.

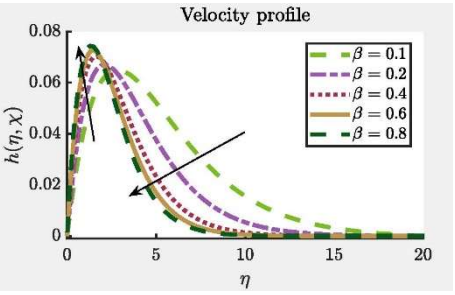

Fig. 15. Profiles of h for different β.

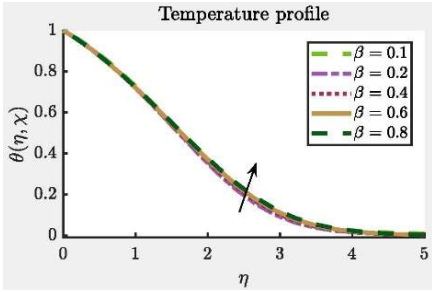

Fig. 16. Variations of θ for different β.

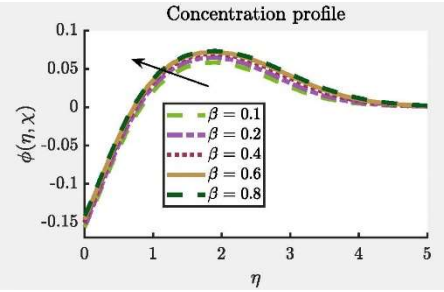

Fig. 17. Variations of ϕ for different β.

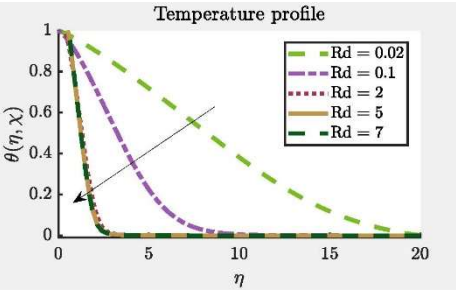

Fig. 18. Variations of θ with *Rd*.

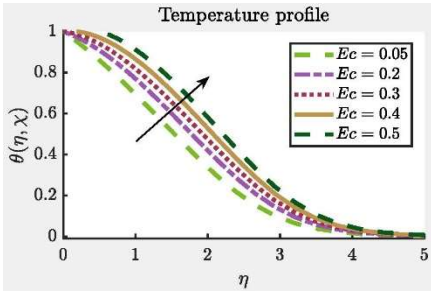

Fig. 19. Variations of ϕ with *Ec*.

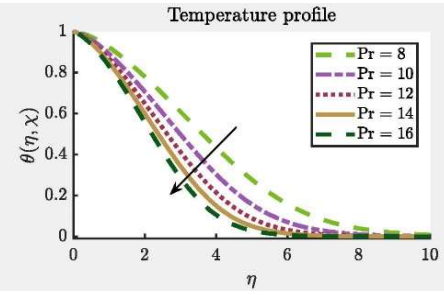

Fig. 20. Influence of *Pr* on θ.

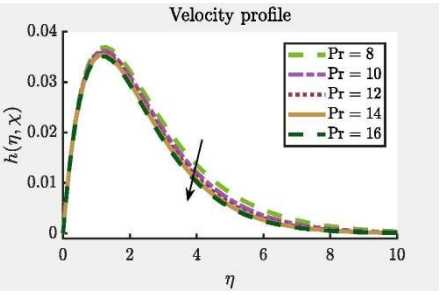

Fig. 21. Behaviour of h for different Pr.

Figure 19 is drawn to highlight the behaviour of temperature field with Eckert number Ec when $M = 2$, $Pr = 15$, $\beta = 0.5$, $m = 0.5$, $p = 0.3$, $Nt = Nb = 0.5$, $Le = 5$, $A^* = B^* = 0.5$, $Nr = 0.5$, $\delta = 0.5$, $Rd = 0.2$ and $\chi = 0.5$. By definition of Eckert number, a positive Ec corresponds to fluid heating (heat is being supplied across the wall into the fluid). There is

considerable increment in fluid temperature with Ec . This increment in fluid temperature is attributed as the internal heat generated due to viscous dissipation in the flow region. Figure 20 presents the dependence of thermal field on Prandtl number Pr. Low Prandtl number Pr refers fluid with large thermal conductivity and this produces thicker thermal boundary layer structures than that for high Prandtl number Pr. From this figure one can immediately notice that fluid temperature decreases with an increase in Pr and this decrease is more pronounced far away from the surface. As a consequence, an increase in the surface temperature gradient occurs. The Pr number has retarding influence on the secondary flow as seen from Fig. 21. Figures 22-25 are sketched to appraise the effects of buoyancy force parameter χ on the primary and secondary flow, fluid temperature and nano particle concentration. A positive χ exerts an assisting pressure gradient that boosts the fluid flow and heat transfer in the boundary layer region. The concerned figures clearly reveal that it promotes the primary as well as secondary flow whereas it declines the fluid temperature and nanoparticle concentration.

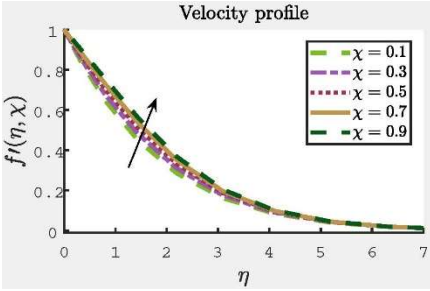

Fig. 22. Profiles of f' for different χ .

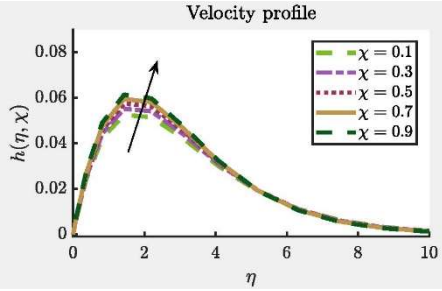

Fig. 23. h profiles for different χ .

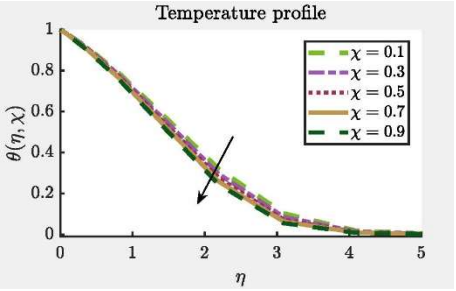

Fig. 24. θ profiles for different χ .

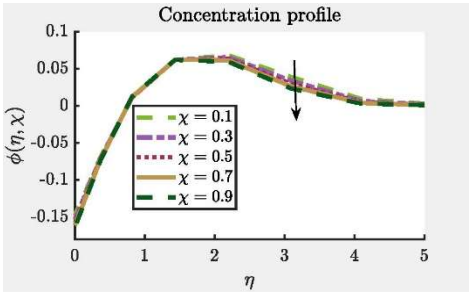

Fig. 25. ϕ profiles for different χ .

Table 1. Variations of skin friction, Nusselt number and Sherwood number for various values of M , Nb, Nt, Rd, with $Pr = 15, Le = 5, p = 0.3, \chi = 0.5, A^* = B^* = 0.5, \beta = 0.5, Ec = 0.1$ and $Nr = 0.5$.

M	Nb	Nt	Rd	$f''(0,\chi)$	$-\theta'(0,\chi)$	$-\phi'(0,\chi)$
1	0.3	0.1	0.2	-0.377030	0.245556	-0.081852
2				-0.579651	0.173937	-0.057979
3				-0.747884	0.115031	-0.038344
4				-0.894203	0.064266	-0.021422
5				-1.024999	0.019319	-0.006440
2	0.05	0.1	0.2	-0.616382	0.166795	-0.333591
	0.1			-0.618213	0.168799	-0.168799
	0.15			-0.618881	0.169437	-0.112958
	0.3			-0.619576	0.170061	-0.056687
	0.5			-0.619862	0.170307	-0.034061
2	0.3	0.05	0.2	-0.581577	0.178789	-0.029798
		0.1		-0.579804	0.173934	-0.057978
		0.15		-0.578048	0.169151	-0.084576
		0.2		-0.576304	0.164442	-0.109628
		0.25		-0.574569	0.159806	-0.133172
2	0.3	0.1	0.02	-0.491486	0.067081	-0.022356
			0.1	-0.546794	0.136432	-0.045478
			2	-0.661667	0.180952	-0.060317
			5	-0.677589	0.087860	-0.029287
			7	-0.678794	0.047883	-0.015961

Table 1 shows the behavioural changes of Skin friction, local Nusselt number and local Sherwood number with magnetic parameter M, Brownian motion parameter Nb, thermophoresis parameter Nt and non-linear radiation parameter Rd. We infer from Table 1 that an increase in magnetic parameter M, results in reduced velocity profiles in the boundary layer which is

depicted by increasing value of Skin friction. On the other hand, it can be observed that the Sherwood number and Nusselt Number decreases. Moreover, increase in Brownian motion parameter *Nb* is directly proportional to the mobility of nanoparticles in the boundary layer region. This fact can be attributed from the increasing trend in the values of both skin friction and Nusselt numbers. Physically, we can say that, the rates of heat transfer in the boundary layer increases significantly with increase in *Nb*. A decrease in skin friction and Nusselt number and an increase in Sherwood number are observed with thermophoresis parameter *Nt*. A mixed behaviour is observed in the values of Nusselt and Sherwood numbers with increase in radiation parameter whereas, the skin friction seems to increase.

5. Conclusion

An analysis on steady mixed convection flow of a Casson nanofluid over a non-linear stretching sheet with Hall current, non-linear radiation and viscous and Joule dissipation are presented. A passively controlled nanoparticle concentration at the surface is considered. The governing non-dimensionalized partial differential equations are traced by a recently developed method known as "Spectral Paired Quasi-linearization method". The convergence and accuracy of the numerical scheme are discussed. Some of the important findings of the present study are:

1. The buoyancy parameter has considerable influence in controlling the flow. The effect of χ is to increase momentum boundary layer thickness and to decrease the thermal and concentration boundary layer.
2. Casson parameter β decreases the primary velocity and increases fluid temperature.
3. Thermal boundary layer is greatly influenced by conduction radiation parameter.
4. The thermal boundary layer grows with Eckert number and thins with Prandtl number.
5. Hall current induces secondary flow. Hall current boosts primary as well as secondary flow.
6. The skin friction increases whereas local Nusselt number and local Sherwood number decrease with the increasing values of *M*.

Acknowledgments

The authors are very much thankful to the unknown reviewers for their valuable and constructive suggestions which improved the readability of the paper.

Conflict of Interest

The author(s) declared no potential conflicts of interest with respect to the research, authorship and publication of this article.

Funding

The author(s) received no financial support for the research, authorship and publication of this article.

Nomenclature

$\bar{\theta}$	dimensional fluid temperature	$\bar{\phi}$	dimensional nanoparticle concentration
β	Casson fluid parameter	β_T	coefficient of thermal expansion
k	thermal conductivity	σ	electrical conductivity
σ^*	Stefan-Boltzmann constant	a_r	Rosseland mean absorption coefficient
υ	kinematic viscosity	ρ	mass density
c_p	specific heat	$(\rho c)_p$	effective heat capacity of the nanoparticle material
$(\rho c)_f$	effective heat capacity of fluid	d_B	Brownian diffusion coefficient
d_θ	thermophoresis diffusion coefficient	$\theta_w (>1)$	surface temperature excess ratio
M	magnetic parameter	Pr	Prandtl number
Nb	Brownian motion parameter	Nt	thermophoresis parameter
Le	Lewis number	Rd	conduction-radiation parameter

References

[1] Turkyilmazoglu, M., Mixed convection flow of magnetohydrodynamic micropolar fluid due to a porous heated/cooled deformable plate: exact solutions, *International Journal of Heat and Mass Transfer*, 106, 2017, 127-134.
[2] Turkyilmazoglu, M., Analytical solutions to mixed convection MHD fluid flow induced by a nonlinearly deformi ng permeable surface, *Communications in Nonlinear Science and Numerical Simulation*, 63, 2018, 373-379.

[3] Shit, G.C., Haldar, R., Combined Effects of Thermal Radiation and Hall Current on MHD Free-Convective Flow and Mass Transfer over a Stretching Sheet with Variable Viscosity, *Journalof Applied Fluid Mechanics*, 5(2), 2012, 113-121.
[4] Salem, A.M., Abd el Aziz, M., Effect of Hall currents and chemical reaction on hydromagnetic flow of a stretching vertical surface with internal heat generation/absorption, *Applied Mathematical Modelling*, 32, 2008, 1236-1254.
[5] Sreedevi, R., Rao, R.R., Prasad Rao, D.R.V., Chamkha, A.J., Combined influence of radiation absorption and Hall current effects on MHD double-diffusive free convective flow past a stretching sheet, *Ain Shams Engineering Journal*, 7(1), 2016, 383-397.
[6] Su, X., Hall and ion-slip effects on the unsteady MHD mixed convection of Cu-water nanofluid over a vertical stretching plate with convective heat flux, *Indian Journal of Pure and Applied Physics*, 55, 2017, 564- 573.
[7] Prasad, K.V., Vajravelu, K., Vaidya, H., Hall Effect on MHD Flow and Heat Transfer over a Stretching Sheet with Variable Thickness, *International Journal Computational Methods in Engineering Science and Mechanics*, 17(4), 2016, 288-297.
[8] Abd el Aziz M., Flow and heat transfer over an unsteady stretching surface with Hall Effect, *Meccanica*, 45(1), 2010, 97-109.
[9] Vajravelu, K., Prasad, K.V., Vaidya, H., Influence of Hall Current on MHD Flow and Heat Transfer over a slender stretching sheet in the presence of variable fluid properties, *Communications in Numerical Analysis*, 2016(1), 2016, 17-36.
[10] Ali, M., Alam, M.S., Soret and Hall effect on MHD flow heat and mass transfer over a vertical stretching sheet in a porous medium due to heat generation, *ARPN Journal of Engineering and Applied Science,* 9(3), 2014, 361-371.
[11] Pal, D., Hall current and MHD effects on heat transfer over an unsteady stretching permeable surface with thermal radiation, *Computers and Mathematics with Applications*, 66(7), 2013, 1161-1180.
[12] Shateyi, S., Marewo, G.T., On a new numerical analysis of the Hall effect on MHD flow and heat transfer over an unsteady stretching permeable surface in the presence of thermal radiation and heat source/sink, *Boundary Value Problems*, 2014, 2014, 170.
[13] Sheikholeslami, M., Rokni, H.B., Effect of melting heat transfer on nanofluid flow in existence of magnetic fiel d considering Buongiorno Model, *Chinese Journal of Physics*, 55(4), 2017, 1115-1126.
[14] Sheikholeslami, M., New computational approach for energy and entropy analysis of nanofluid under the impact of Lorentz force through a porous media, *Computer Methods in Applied Mechanics and Engineering*, 344, 2019, 319-333.
[15] Sheikholeslami, M., Shehzad, S.A., Li, Z., Shafee, A., Numerical modeling for alumina nanofluid magnetohydrodynamic convective heat transfer in a permeable medium using Darcy law, *International Journal of Heat and Mass Transfer*, 127, 2018, 614-622.
[16] Sheikholeslami, M., Rokni, H.B., Magnetic nanofluid flow and convective heat transfer in a porous cavity considering Brownian motion effects, *Physics of Fluids,* 30(1), 2018, 012003.
[17] Sheikholeslami, M., Application of Darcy law for nanofluid flow in a porous cavity under the impact of Lorentz forces, *Journal of Molecular Liquids,* 266, 2018, 495-503.
[18] Sheikholeslami, M., Numerical approach for MHD Al_2O_3-water nanofluid transportation inside a permeable medium using innovative computer method, *Computer Methods in Applied Mechanics and Engineering,* 344, 2019, 306-318.
[19] Sheikholeslami, M., Numerical investigation of MHD nanofluid free convective heat transfer in a porous tilted enclosure, *Engineering Computations,* 34(6), 2017, 1939-1955.
[20] Turkyilmazoglu, M., Buongiorno Model in a nanofluid filled asymmetric channel fulfilling zero net particle flux at the walls, *International Journal of Heat and Mass Transfer*, 126, 2018, 974-979.
[21] Abd el-Aziz, M., Effects of Hall current on the flow and heat transfer of a nanofluid over a stretching sheet with partial slip, *International Journal of Modern Physics C*, 24(7), 2013, 1350044.
[22] Su, X., Zheng, L., Hall effect on MHD flow and heat transfer of nanofluids over a stretching wedge in the presence of velocity slip and Joule heating, *Central European Journal of Physics*, 11(12), 2013, 1694-1703.
[23] Abdel-Wahed, M., Akl, M., Effect of hall current on MHD flow of a nanofluid with variable properties due to a rotating disk with viscous dissipation and nonlinear thermal radiation, *AIP Advances*, 6, 2016, 095308.
[24] Makinde, O.D., Iskander, T., Mabood, F., Khan, W.A., Tshehla, M.S., MHD Couette- Poiseuille flow of variable viscosity nanofluids in a rotating permeable channel with Hall effects, *Journal of Molecular liquids*, 221, 2016, 778-787.
[25] Hayat, T., Shafique, M., Tanveer, A., Alsaedi, A.,Hall and ion slip effects on peristaltic flow of Jeffrey nanofluid with Joule heating,*Journal of Magnetism and Magnetic Materials*, 407, 2016, 51.
[26] Gireesha, B.J., Mahanthesh, B., Krupalakshmi, K.L., Hall effect on two- phase radiated flow of magneto-dusty-nanoliquid with irregular heat generation/ consumption, *Results in Physics*, 7, 2017, 4340-4348.
[27] Ullah, I., Bhattacharyya, K, Shafie, S., Khan, I., Unsteady MHD Mixed Convection Slip Flow of Casson Fluid over Nonlinearly Stretching Sheet Embedded in a Porous Medium with Chemical Reaction, Thermal Radiation, Heat Generation/ Absorption and Convective Boundary Conditions, *PLoS ONE,* 11(10), 2016, e0165348.
[28] Nadeem S., Ul Haq, R., Akbar, N.S., MHD three-dimensional boundary layer flow of Casson nanofluid past a linearly stretching sheet with convective boundary condition, *IEEE Transactions on Nanotechnology*, 13, 2014, 109-115.
[29] Hussain, T., Shehzad, S.A., Alsaedi, A., Hayat, T., Ramzan, M., Flow of Casson nanofluid with viscous dissipation and convective conditions: a mathematical model, *Journal of Central South University*, 22, 2015, 1132-1140.
[30] Mustafa, M., Khan, J. A., Model for flow of Casson nanofluid past a non-linearly stretching sheet considering magnetic field effects, *AIP Advances*, 5, 2015, 077148.
[31] Ullah, I., Khan, I. Shafie, S., MHD Natural Convection Flow of Casson Nanofluid over Nonlinearly Stretching Sheet Through Porous Medium with Chemical Reaction and Thermal Radiation, *Nanoscale Research Letters*, 11, 2016, 527.

[32] Ibrahim, W., Makinde, O.D., Magnetohydrodynamic Stagnation Point Flow and Heat Transfer of Casson Nanofluid Past a Stretching Sheet with Slip and Convective Boundary Condition, *Journal of Aerospace Engineering*, 29(2), 2016, 04015037.
[33] Sulochana, C., Ashwinkumar, G.P., Sandeep, N., Similarity solution of 3D Casson nanofluid flow over a stretching sheet with convective boundary conditions, *Journal of Nigerian Mathematical Society*, 35, 2016, 128-141.
[34] Hayat, T., Aziz, A., Muhammad, T., Alsaedi, A., Active and passive controls of Jeffrey nanofluid flow over a nonlinear stretching surface, *Results in Physics*, 7, 2017, 4071-4078.
[35] Cowling, T. G., *Magnetohydrodynamics*, Interscience, New York, 1957.
[36] Kuznetsov, A.V., Nield, D.A., Natural convective boundary-layer flow of a nanofluid past a vertical plate, *International Journal of Thermal Sciences*, 49, 2010, 243-247.
[37] Rahman, M.M., Eltayeb, I.A., Radiative heat transfer in a hydromagnetic nanofluid past a non-linear stretching surface with convective boundary condition, *Meccanica*, 48, 2013, 601-615.
[38] Gireesha, B.J., Krishnamurthy, M.R., Prasannakumara, B.C., Gorla, R.S.R., MHD flow and non-linear radiative heat transfer of a Casson nanofluid past a nonlinearly stretching sheet in the presence of a chemical reaction, *Nanoscience and Technology: An International Journal*, 9 (3), 2018, 207-229.
[39] Hayat, T., Qayyum, S., Alsaedi, A., Asghar, S., Radiation effects on the mixed convection flow induced by an inclined stretching cylinder with non-uniform heat source/sink, *PLoS One*, 12(4), 2017, e0175584.
[40] Motsa, S.S., Animasaun, I.L., Paired quasi-linearization analysis of heat transfer in unsteady mixed convection nanofluid containing both nanoparticles and gyrotactic microorganisms due to impulsive motion, *Journal of Heat Transfer*, 138(11), 2016, 114503.
[41] Otegbeye, O., Motsa, S.S., A paired quasilinearization method for solving boundary layer flow problems, *AIP Conference Proceedings*, 1975(1), 2018, 030020.
[42] Bellman, R.E., Kalaba, R.E., *Quasilinearisation and non-linear boundary-value problems*, Elsevier, New York, 1965.
[43] Boyd, J.P., *Chebyshev and Fourier spectral methods*, Dover Publications, 2001.
[44] Trefethen, L.N., *Spectral methods in MATLAB*, SIAM, 10th ed., 2000.
[45] Canuto, C., Husseini, M.Y., Quarteroni, A., Zang, T.A., *Spectral Methods in Fluid Dynamics*, Springer-Verlag, Berlin, 1988.